


# Structural, electronic, and magnetic properties of $\text{Fe}_x\text{Co}_y\text{Pd}_z$ ( $x + y + z \leq 7$ ) clusters: a density functional theory study

Alejandro Varas · F. Aguilera-Granja ·  
José Rogan · Miguel Kiwi 

Received: 13 April 2016 / Accepted: 3 August 2016 / Published online: 23 August 2016  
© Springer Science+Business Media Dordrecht 2016

**Abstract** Transition metal alloy nanoparticles are of interest both theoretically and experimentally, particularly due to their potential technological applications, and to their novel structural and magnetic properties in the subnanometer region. Here we compute structural parameters, chemical and magnetic properties, and the fragmentation channels of  $\text{Fe}_x\text{Co}_y\text{Pd}_z$  nanoparticles, for  $x + y + z \leq 7$ , and compare our results with macroscopic systems whenever it is feasible. We carry out density functional theory calculations, as implemented in the SIESTA code, for all possible concentrations (i.e., all  $x$ -,  $y$ -, and  $z$ -values). The seeds for the possible homotops are built using a semiempirical Gupta potential; these, and additional low coordinated conformations, are thereafter subject to

reoptimization by means of the SIESTA code. To the best of our knowledge, this is the first time that such kind of calculations are performed for all the possible compositions of up to 7 atom ternary nanoclusters. We find that the binding is strongest in the FeCo-rich region and weakest for pristine Pd for all the sizes we considered. Interatomic distances in general decrease monotonically, as the FeCo region is approached. The total magnetic moment varies almost continuously over the composition range, with the large Fe moment being quenched by the addition of Pd and/or Co; however, an almost continuous range of the moments magnitude can be achieved, which allows for fine tuning magnetism by controlling the composition. As far as the fragmentation channels are concerned, for neutral, cationic, and anionic clusters, the most likely path is through atomic  $\text{Pd}^0$ ,  $\text{Pd}^+$ , and  $\text{Pd}^-$ , when Pd is present in the cluster. However, in the absence of Pd,

**Electronic supplementary material** The online version of this article (doi:10.1007/s11051-016-3554-3) contains supplementary material, which is available to authorized users.

A. Varas · J. Rogan · M. Kiwi  
Departamento de Física, Facultad de Ciencias,  
Universidad de Chile, Casilla 653, Santiago 7800024,  
Chile

A. Varas  
Nano-Bio Spectroscopy Group and ETSF Scientific  
Development Centre, Departamento de Física de  
Materiales, Universidad del País Vasco UPV/EHU, Av.  
Tolosa 72, 20018 San Sebastián, Spain

F. Aguilera-Granja  
Instituto de Física, Universidad Autónoma de San Luis  
Potosí, 78000 San Luis Potosí, Mexico

F. Aguilera-Granja  
DIPC Donostia International Physics Center,  
20018 San Sebastián, Spain

J. Rogan · M. Kiwi (✉)  
Centro para el Desarrollo de la Nanociencia y la  
Nanotecnología (CEDENNA), Avda. Ecuador 3493,  
Santiago 9170124, Chile  
e-mail: m.kiwi.t@gmail.com

the most likely fragmentation channel is through the majority element. Molecular fragmentation channels are only observed for very small cluster sizes.

**Keywords** Metallic nanoclusters · Magnetic clusters · Modeling and simulations

## Introduction

Nanoclusters of several atomic elements (mainly binaries and ternaries), have recently attracted significant interest due to several reasons: on the one hand nanoclusters are of interest for applications, as they offer the possibility of generating novel material properties, significantly different from the bulk, which could be used in electronics, catalysis, and magnetic devices. On the other hand, since nanoclusters “behave as composite entities, which mimic the properties of some element atoms and yet retain their integrity” (Castleman 2011), they have given birth to the concept of “superatoms.” Moreover, the purpose of creating novel materials led to intense efforts to develop and understand the behavior of ternary alloys, as reflected in an 18 volume encyclopedia on the subject (Petzow and Effenberg 1989).

During some time, binary nanoclusters have been studied theoretically both using semiclassical and ab initio methods (Lee et al 1997, 2003, 2006; Rogan et al. 2013a, b; Muñoz et al. 2013a, b). Lately, the size of the nanoclusters that can be handled by means of density functional theory (DFT) techniques has gradually increased, as computer power and availability steadily grows. In particular, ternary nanoclusters have been investigated with different classical techniques for some time (Rubinovich and Polak 2004; Polak and Rubinovich 2005; Fallah et al. 2013). Nevertheless, DFT work on ternaries has also been reported lately (Guzmán-Ramírez et al. 2011, 2013; Miralrio and Sansores 2014), but the literature on them is by far not as abundant as for their binary counterparts (Ferrando et al. 2008).

We focus on the electronic, structural, and magnetic properties of heteroatomic transition metal nanoclusters, with the general objective of obtaining some knowledge about properties that could prove useful for technological applications. We are well aware that our studies are limited to the subnanometer regime, and

that simple extrapolations of our results are not necessarily reliable. Nevertheless, some general tendencies can be derived. Homoatomic clusters only allow to modify their size, in order to modify their total magnetic moment, by changes of coordination, interatomic distances, and symmetry (Billas et al. 1994; Sun et al. 2000; Knickelbein 2001). However, if the nanoscale equivalent of alloying is implemented, that is the formation of heteroatomic clusters, then the feasibility of tuning magnetic properties is enhanced. Fe, Co, and Ni nanoclusters are elements of interest because of their parallel magnetic coupling, enhanced magnetic moments relative to the bulk, and compact conformations. This motivated (Guzmán-Ramírez et al. 2011, 2013) to investigate some selected  $\text{Fe}_x\text{Co}_y\text{Ni}_z$  structures, and their homotops. On the other hand, Ni and Pd atoms have some similar electronic properties but differ slightly in atom size, but to the best of our knowledge, no theoretical studies on ternary  $\text{Fe}_x\text{Co}_y\text{Pd}_z$  nanoalloys, that cover the whole concentration range, have yet been reported.

Here we investigate, by means of DFT, the minimal-energy geometrical conformations, their interatomic distances, chemical order, vertical ionization potential, vertical electron affinity, and magnetic moments of ternary  $\text{Fe}_x\text{Co}_y\text{Pd}_z$  clusters, for  $x + y + z \leq 7$ . We also study the fragmentation channels of their neutral, cationic, and anionic structures.

This paper is organized as follows: after this introduction we provide details of the model and the computational procedure in “[Details of the computational procedure and model](#)” section. Next, in “[Results](#)” section, we present results for the nanocluster geometries, interatomic distances, energy, chemical order, ionization potential, electron affinity, and magnetic moments. Finally, we report the fragmentation channels of their neutral, cationic, and anionic structures. In “[Conclusions](#),” we draw conclusions and close the paper.

## Details of the computational procedure and model

Our calculations were performed using the SIESTA DFT package (Soler et al. 2002), which employs numerical pseudoatomic orbitals as basis sets to solve the single-particle Kohn–Sham equations. In this work, we used the Perdew–Burke–Ernzerhof form of the generalized gradient approximation (GGA) for the

exchange and correlation potential (Perdew et al. 1996), and the atomic cores were described by nonlocal norm-conserving scalar-relativistic Troullier–Martins pseudopotentials (Troullier and Martins 1991), factorized in the Kleinman–Bylander form Kleinman and Bylander (1982). The pseudopotentials for Fe and Co were generated using the valence configurations  $4s^1 4p^0 3d^n$  with  $n=7$  and 8, respectively, where as for Pd,  $5s^1 5p^0 4d^n$ , with  $n = 9$  is used. The  $s$ ,  $p$ , and  $d$  cutoff radii were 2.00, 2.00, and 2.00 a.u. for Fe; 2.05, 2.05, and 2.05 for Co; and 2.27, 2.45, and 1.66 a.u. for Pd. We have included nonlinear core corrections with a matching radius of 0.70 a.u. for Fe, 0.75 a.u. for Co, and 1.20 a.u. for Pd, respectively. We confirmed that these pseudopotentials accurately reproduce the eigenvalues of the different excited states of the respective isolated atoms. The valence states were described using a double- $\zeta$  doubly polarized basis set.

An electronic temperature of 25 meV for smearing, and a 250 Ry energy cutoff to define the real-space grid for numerical calculations involving the electron density was implemented. We have tested larger cutoffs and lower electronic temperatures for some particular cases, and verified that they do not substantially modify the results. To optimize the geometrical structures, we performed a local relaxation using the conjugate gradient algorithm (Press et al. 1992), starting from a variety of initial structures previously generated with a semiempirical Gupta potential (Gupta 1981; Cleri and Rosato 1993), since these geometries have different symmetries and different spin configurations, which are incorporated in our search of putative energy minima. The structural optimization was finalized when each force component, on every atom in the cluster, was smaller than 6 meV/Å. In the calculations, the clusters were placed in a supercell  $20 \times 20 \times 20 \text{ \AA}^3$  in size, large enough to insure that (a) the interaction between the cluster and its replicas in neighboring cells is negligible; and (b) that it is sufficient to consider just the  $\Gamma$  point ( $k = 0$ ) when integrating over the Brillouin zone. More details about the reliability of the pseudopotentials and basis sets used, as well as about the pertinent tests that we carried out, can be found in the literature (Aguilera-Granja et al. 2008, 2013). In order to test the validity of the pseudopotentials we used, we calculated the binding energy and the interatomic distance of the

metal dimers studied here as a benchmark (see Supporting Information).

In this contribution, we investigate all the local minima generated by a semiempirical Gupta potential (Cleri and Rosato 1993; Gupta 1981) search for  $N \leq 7$ , using the strategy developed by Rogan et al. (2013b), which has been successfully employed in several recent publications (Muñoz et al. 2013a, b; Rogan et al. 2013a; Varas et al. 2015; Munoz et al. 2015). Later on, the resulting structures are reoptimized using the SIESTA code to include the possibility of different energy ordering of the various homotops and isomers, as well as accurate structures at a DFT level. Since the Gupta potential is prone to generate highly coordinated structures, it is worth pointing out that some low coordination structures were also included.

The parameters corresponding to the homonuclear Fe–Fe Guillopé and Legrand (1989), Co–Co Cleri and Rosato (1993), and Pd–Pd Cleri and Rosato (1993), interactions are summarized in Table 1.

The parameters for the heterogeneous Fe–Co, Fe–Pd, and Co–Pd interactions were obtained as the geometric averages of the homonuclear parameters.

## Results

All the structural, chemical, and magnetic parameters that we computed are summarized in Tables S8 to S12, for  $3 \leq N \leq 7$  (see Supporting Information).

### Geometry

For the  $N = 5$  case (top panel of Fig. 1), we observe only two different structures: hexahedral (in two versions: a regular and an irregular shape), and a square pyramid (also regular and distorted, depending on the composition). Only a few pyramids are located

**Table 1** Parameters corresponding to the homonuclear Fe–Fe, Co–Co, and Pd–Pd interactions on the Gupta potential

Interaction	$A$ [eV]	$\zeta$ [eV]	$p$	$q$	$r^0$ [Å]
Fe–Fe	0.13315	1.6179	10.50	2.60	2.553
Co–Co	0.0950	1.4880	11.604	2.286	2.497
Pd–Pd	0.1746	1.718	10.867	3.742	2.749

**Fig. 1** Conformations of the  $\text{Fe}_x\text{Co}_y\text{Pd}_z$  nanoalloys, for  $x + y + z = 5$  (top panel),  $x + y + z = 6$  (center panel), and  $x + y + z = 7$  (bottom panel)

near to the composition-triangle corners. In the particular case of  $\text{Fe}_5$ , both structures (symmetric hexahedral and perfect pyramid) are degenerate. Our results agree well with the work done by Ramírez and coworkers for the (FeCo) binary system using Gaussian03, the only exception being  $\text{Co}_4\text{Fe}$  where we obtain a pyramid, whereas Ramírez et al. (2011) propose an hexahedral cluster.

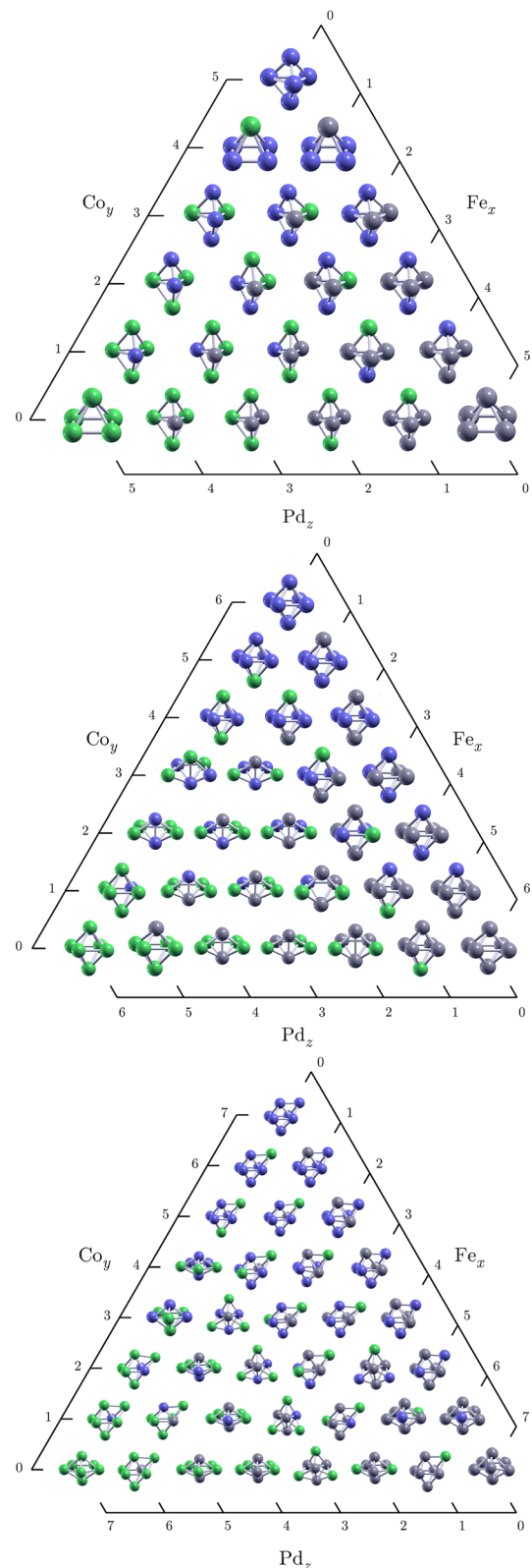
For  $N = 6$ , only two structures are present (middle panel of Fig. 1): octahedral and distorted decahedral-like (decahedral with one atom missing) for Pd concentrations  $2 \leq z \leq 4$ , with the octahedral one being the most frequent structure. In general, our calculations for the binary (FeCo) system agree fairly well with those by Guzmán-Ramírez et al. (2013) for the different homotops (since the octahedral structure is observed over the whole range). When differences are present, the different homotops are practically energy degenerate.

For  $N = 7$  three different structures are present (bottom panel of Fig. 1): capped octahedral, distorted decahedral, and three capped tetrahedra (cited in decreasing frequency order). The decahedral is observed mainly along the line with four Pd atoms, in the binary system of (FePd) and in the corner of the Fe-rich zone. The capped tetrahedra is observed particularly along the three Pd atoms line, and for  $\text{Fe}_4\text{Co}_2\text{Pd}$ . Our calculation for binary (FeCo) system agree well with previous work; when differences are observed it turns out that the structures are practically degenerate (Guzmán-Ramírez et al. 2013).

Our results for CoPd agree partially with Cantera-López et al. (2010) for  $N = 5$  and 7, since in their work is limited to different decorations (homotops) of triangles, hexahedra, and decahedral structures. We also agree partially with recent results by Mokkath et al. (2014) using the VASP code with LDA and GGA for CoPd, and some coincidence is also observed for FePd impurities calculations by Ma et al. (2013) using the DMOL computational package with GGA and PW91.

#### Interatomic distances

The bulk nearest-neighbor distances, at room temperature and pressure, of Fe, Co, and Pd are 2.54, 2.50, and 2.76 Å, respectively (Kittel 1996). However,



when they form nanoclusters these values change significantly. In Fig. 2, we illustrate the average interatomic distances (AID) of the clusters. As is expected, the largest values of the AID's are found in the Pd-rich region, which in the bulk has the largest nearest-neighbor (nn)-distance. In general, the smallest values of the AID are observed in the Co-rich

region, and are related to the different structures. For the sizes considered, it is not possible to observe a one-to-one correspondence between the AID's with the different structures, the only exception being  $N = 4$  (see Supporting Information).

In general, the average interatomic distance (AID) grows almost monotonously with the number of Pd atoms in the cluster, mainly due to the different atomic radii (or larger number of core electrons) of Pd as compared with Fe and Co. The AID for all the sizes here considered decreases when Fe and Co are added to the cluster, the shortest ones occur when Co is the richest component. Our results for AID values and geometric structures are similar to the ones reported by Ramírez et al. using GAUSSIAN for  $N = 5, 6,$  and  $7$  (Guzmán-Ramírez et al. 2011, 2013) FeCo nanoclusters, and are also similar to ones reported by the results by Cantera-López et al. ((2010) using SIESTA for CoPd clusters with  $N = 5$  and  $7$ ). The few differences are mainly due to the fact that Cantera's work is limited to different decorations (homotops) of triangles, hexahedra, and decahedral structures, and not to a wide minima search Cantera-López et al. (2010). Partial agreement of our results is found for FePd binary systems for  $N = 7$  geometries and distances with work by Montejano-Carrizales et al. (2011) due to the fact that they only consider homotops with decahedral structure, and this structure is not present over the entire composition range. The AID values reported here for all sizes are in fair agreement within the ones in the literature for the binary systems (FeCo, FePd, CoPd); however, we are not aware of any other work on ternaries. In general, the cluster interatomic distances we study are slightly different from the bulk ( $\sim 5\%$ ). As expected, the dimmers are the ones that shrink most ( $\sim 20\%$ ).

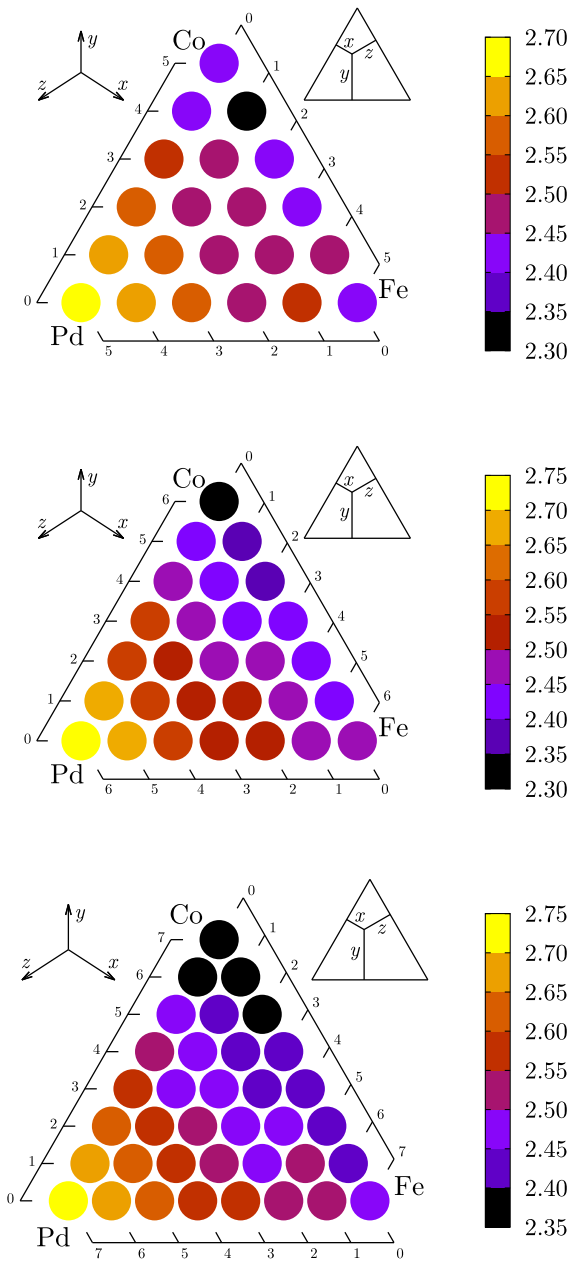


**Fig. 2** Average interatomic distance (AID) in Å of the  $\text{Fe}_x\text{Co}_y\text{Pd}_z$  nanoalloys, for  $x + y + z = 5$  (top panel),  $x + y + z = 6$  (center panel), and  $x + y + z = 7$  (bottom panel)

### Energy

The binding energy per atom  $E_b$  and the excess energy per atom  $E_{exc}$  are defined as follows:

$$E_b(\text{Fe}_x\text{Co}_y\text{Pd}_z) = \frac{E_{\text{Total}}(\text{Fe}_x\text{Co}_y\text{Pd}_z) - xE_{\text{atom}}(\text{Fe}) - yE_{\text{atom}}(\text{Co}) - zE_{\text{atom}}(\text{Pd})}{N}, \tag{1}$$

$$E_{exc}(\text{Fe}_x\text{Co}_y\text{Pd}_z) = E_b(\text{Fe}_x\text{Co}_y\text{Pd}_z) - x \frac{E_b(\text{Fe}_N)}{N} - y \frac{E_b(\text{Co}_N)}{N} - z \frac{E_b(\text{Pd}_N)}{N}, \tag{2}$$



where  $N = x + y + z$ .

A large binding energy constitutes a measure of the stability of the cluster against the removal of a single, or 1, of its atoms. The cluster excess energy is the energy difference relative to pure systems. Therefore, when  $E_{exc} < 0$  it constitutes an indication of the tendency toward mixing of the different elements.

In Fig. 3 for  $N = 5 \leq N \leq 7$  a monotonous increase of  $E_b$  is observed when moving from Pd to Fe and Co; and a very smooth decrease of  $E_b$  when moving from Co to Fe, which is slightly stronger near the Fe-rich corner. The largest values (the most negative ones, and therefore the more stable ones) are observed in the Fe and Co-rich region, particularly for Fe and for all  $N$  values. It is worth noticing that for  $N = 5$  a meaningful stability increment is observed as the first Co or Fe atom is introduced in the cluster. This also occurs for  $N = 3$  and  $N = 4$  (see Supporting Information).

As far as  $E_{exc}$  is concerned, the largest mixing tendency is observed along the FePd edge, with the largest values for almost equiatomic concentration. For  $N = 7$ , the largest tendency to mixing is only observed close to the Pd-rich corner, but this tendency is also present when Co is introduced in the ternary alloy (bottom panel of Fig. 4). The same  $E_{exc}$  behavior is also observed for  $N = 5$  and  $N = 6$ , with deviations due to size effects (top and middle panel of Fig. 4). The binary CoPd and FeCo have a limited tendency to mixing. However, for these systems as soon as the third component is added, the mixing strongly increases. In general, the weakest tendency to mixing is observed along the CoPd edges, for all sizes.

In Fig. 5, we display results for the second differences  $\Delta_E$ , defined by Eq. (3). The  $\alpha$  index labels the sum over the possible “composition neighbors” of  $\text{Fe}_x\text{Co}_y\text{Pd}_z$ , which means that if the cluster is of just one of the elements (triangle corners) then there are only two neighbors ( $\alpha = 2$ ). If two elements are present (triangle edges) there are four neighbors ( $\alpha = 4$ ), and if the cluster contains all three elements the number of composition neighbors is six ( $\alpha = 6$ ).

$$\Delta_E(\text{Fe}_x\text{Co}_y\text{Pd}_z) = \frac{1}{\alpha} \sum_{i=1}^{\alpha} [E_b(\text{Fe}_x\text{Co}_y\text{Pd}_z)_i - E_b(\text{Fe}_x\text{Co}_y\text{Pd}_z)] . \quad (3)$$

The second difference  $\Delta_E$  is a useful parameter to determine cluster stability against the replacement of an element by a different one Bonačić-Koutecký et al.

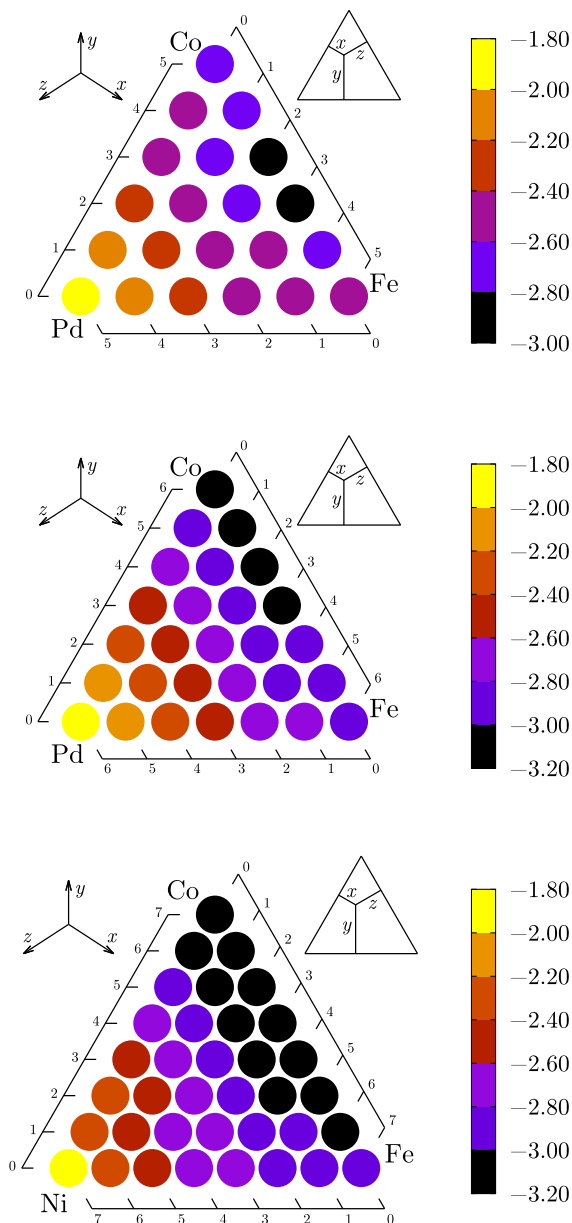


**Fig. 3** Binding energy  $E_b$  of the  $\text{Fe}_x\text{Co}_y\text{Pd}_z$  nanoalloys, for  $x + y + z = 5$  (top panel),  $x + y + z = 6$  (center panel), and  $x + y + z = 7$  (bottom panel)

(1991). Positive  $\Delta_E$  values imply that a certain structure, with a given composition  $(x,y,z)$ , is more stable than the neighboring ones, with possible compositions  $(x, y \pm 1, z \mp 1)$ ,  $(x \pm 1, y \pm 1, z)$ , and  $(x \pm 1, y \mp 1, z)$ . Negative values of  $\Delta_E$  indicate that the substitution process of one element  $(x,y,z)$  can easily take place. A positive value of  $\Delta_E$  constitutes an

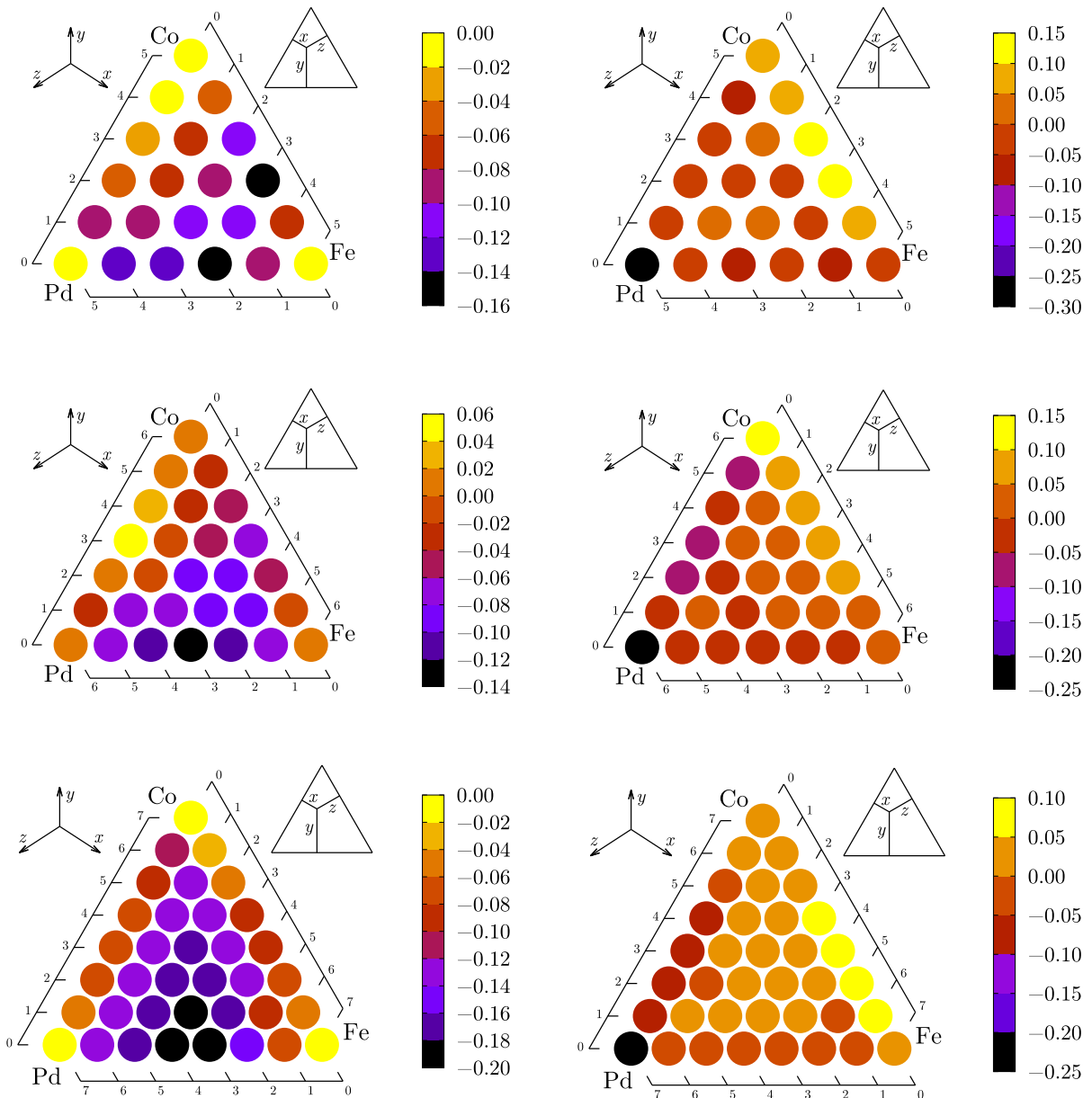


**Fig. 4** Excess energy  $E_{exc}$  of the  $Fe_xCo_yPd_z$  nanoalloys, for  $x + y + z = 5$  (top panel),  $x + y + z = 6$  (center panel), and  $x + y + z = 7$  (bottom panel)

**Fig. 5** (color online) Second energy difference  $\Delta_E$  in eV, of the  $Fe_xCo_yPd_z$  nanoalloys, for  $x + y + z = 5$  (top panel),  $x + y + z = 6$  (center panel), and  $x + y + z = 7$  (bottom panel)

indication that the interchange of one element by another is energetically less favorable.

In Fig. 5, we present the results for  $5 \leq N \leq 7$ , and notice that only the FeCo edges are most prone to keep their composition, and are more stable as far as chemical composition is concerned. This trend changes as soon as Pd is introduced, and the most prone structures to change its compositions are located

in the Pd-rich corner. The same behavior is also observed for  $N = 3$  and  $N = 4$  (see Supporting Information).

#### Chemical order

For multicomponent nanoalloys their finite size makes the definition of chemical order (segregation or

mixing) quite difficult. In order to analyze analytically these trends, as a function of composition, it is convenient to define the order parameter  $\sigma$ , with the following characteristics: positive when phase-separation or segregation takes place, negative when mixing is present, and  $\approx 0$  at the segregation to mixing transition. The parameter  $\sigma \approx 0$  identifies a disordered phase, although for finite systems this phase and the mixed one are quite similar. The order parameter  $\sigma$ , generally used in bulk-like binary alloy systems, was introduced by Ducastelle Ducastelle (1991), and it allows to distinguish between disorder ( $\sigma \approx 0$ ) and mixing (small negative  $\sigma$  values), but it also allows to characterize other ordered phases, like the layered-like phases (large  $-\sigma$  values).

In our case, the  $\sigma$  parameter is defined as follows:

$$\sigma = \frac{N_{\text{Fe-Fe}} + N_{\text{Co-Co}} + N_{\text{Pd-Pd}} - N_{\text{Fe-Co}} - N_{\text{Co-Pd}} - N_{\text{Fe-Pd}}}{N_{\text{Fe-Fe}} + N_{\text{Co-Co}} + N_{\text{Pd-Pd}} + N_{\text{Fe-Co}} + N_{\text{Co-Pd}} + N_{\text{Fe-Pd}}}, \quad (4)$$

where  $N_{A-B}$  is the number of nearest-neighbor  $A-B$  bonds. Therefore, this parameter is based on the short-range order correlations, which are the most important ones for transition metal systems. The number of these different kinds of nearest-neighbor bonds depends on the different structures and compositions, and has to be calculated separately for each case of interest.

Segregation is observed close to the corners of Fig. 6, that is in the region where the cluster is either pure, or when one of the three elements predominates. Segregation is particularly noticeable in the Fe and Pd-rich corners for  $N = 5$ , and in the Fe, Co, and Pd corners, for  $N = 6$ , and the Fe and Co corners for  $N = 7$ . The most negative values of  $\sigma$  are associated with a tendency of the system to form layered configurations. Almost all the central regions within the triangles show this behavior, as well as the edges: CoPd and FePd for  $N = 5$ , all edges for  $N = 6$ , and FeCo and FePd for  $N = 7$ . This tendency to form ABA layers may be due to the very small size of the cluster, and the large size difference between Pd, Fe, and Co atoms, which try to avoid Pd, and prefer that Pd be close to other Pd atoms to form alternate pairs. Similar results are observed for the FeCoNi ternary alloys reported by Guzmán-Ramírez and coworkers (Guzmán-Ramírez et al. 2011, 2013).

The bulk phase diagrams of these alloys are far more complex than the subnanometer clusters we

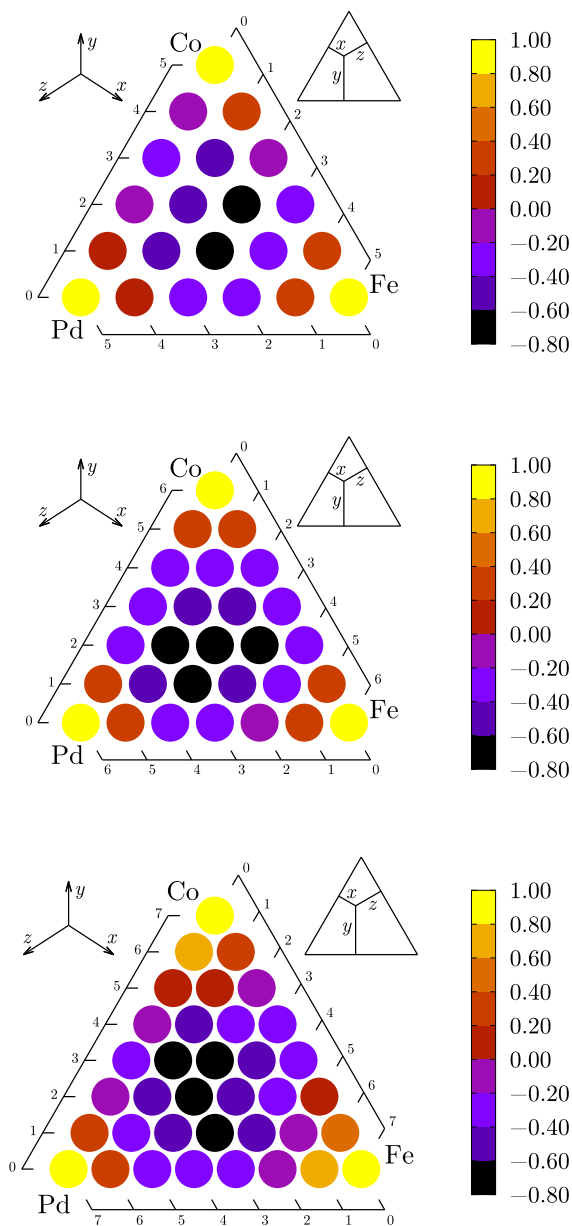


**Fig. 6** (color online) Chemical order parameter  $\sigma$  of the  $\text{Fe}_x\text{Co}_y\text{Pd}_z$  nanoalloys, for  $x + y + z = 5$  (top panel),  $x + y + z = 6$  (center panel), and  $x + y + z = 7$  (bottom panel)

study here, mainly due to the fact that bulk Fe (bcc), Co (hcp), and Pd (fcc) adopt different spatial long-range order and structural transitions as a function of concentration are expected, particularly in one element-rich concentration regions. For Fe-Co alloys, several ordered phases are observed with structural transitions in the Co-rich region (Martínez-Herrera et al. 1985; Sourmail 2005; Massalski et al. 1990). In



Fe-Pd alloys, different phases do coexist and show, particularly for nearly equiatomic concentrations. Fe-Pd alloys are found in the  $L1_0$  phase; for the Fe-Pd<sub>3</sub> alloy the  $L1_2$  phase is present (Massalski et al. 1990; Wakeham et al. 2016) and for Co-Pd alloys different fcc and hcp disordered phases are observed (Martienssen and Warlimont 2005).

However, phases similar to the bulk ones are practically impossible to identify in nanoclusters, due to the tiny size they have. In fact, the only way to characterize them is by using a phenomenological description of the chemical order, which mainly depends on the concentration and the number of atom pairs in the system, as proposed by Ducastelle (1991) and as we have calculated above. Experimentally, core-shell structures are observed in the nano regime (7 nm to 22 nm) for Co@Fe and Co@Pd Ferrando et al. (2008). But we have not been able to find experimental results for FePd.

Vertical ionization potential and vertical electron affinity

The vertical ionization potential (VIP) and the vertical electron affinity (VEA) are defined as

$$VIP = E_{Fe_xCo_yPd_z^+} - E_{Fe_xCo_yPd_z} \tag{5}$$

$$VEA = E_{Fe_xCo_yPd_z} - E_{Fe_xCo_yPd_z^-} \tag{6}$$

When the geometry of the charged species is not allowed to relax, after the electron is added or removed, the above quantities are named vertical IP (VIP) and vertical EA (VEA).

The VIP changes from size to size in our calculations, as is shown in Fig. 7. For  $N = 5$ , their largest values are found along the lines of Pd<sub>0</sub> (excluding pure Fe), Pd<sub>1</sub>, and also for the Co<sub>3</sub>Pd<sub>2</sub>, Pd<sub>5</sub>, and Pd<sub>4</sub>Co clusters. The lowest values are observed for Fe<sub>3</sub>Pd<sub>2</sub>, Fe<sub>2</sub>Pd<sub>3</sub>, FePd<sub>4</sub>, and CoPd<sub>3</sub>. For  $N = 6$  the larger values are near the Co corner as well as for Pd<sub>6</sub> and FePd<sub>5</sub>. The lowest ionization values correspond to FeCo<sub>2</sub>Pd<sub>3</sub>, Fe<sub>2</sub>Pd<sub>4</sub>, Fe<sub>2</sub>CoPd<sub>3</sub>, and Fe<sub>3</sub>Pd<sub>3</sub>. The rest of the configurations has ionization values within the range of 6.4 eV to 6.7 eV. For  $N = 7$  the largest values are located in the Pd<sub>1</sub>, Pd<sub>2</sub>, Pd<sub>3</sub>, and Pd<sub>4</sub> bands, excluding the region very near the Fe-rich corner. Also, pure Pd has a large VIP value. In general, and regardless of size, Pd shows large VIP values, whereas Fe shows smaller ones.

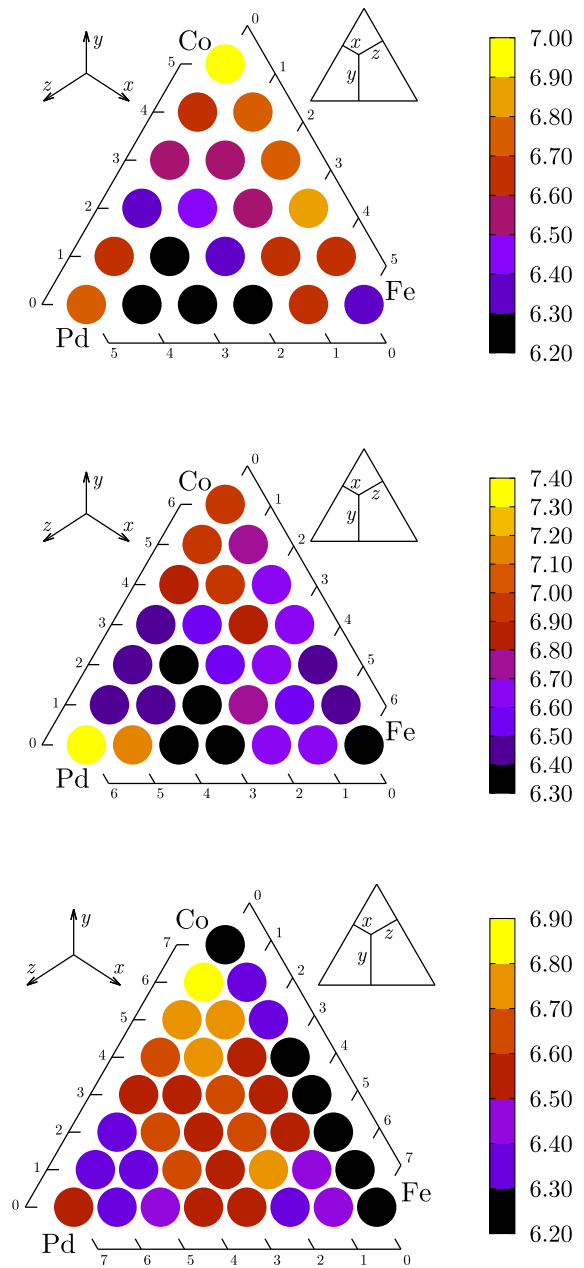


**Fig. 7** Vertical Ionization Potential (VIP) of the  $Fe_xCo_yPd_z$  nanoalloys, for  $x + y + z = 5$  (top panel),  $x + y + z = 6$  (center panel), and  $x + y + z = 7$  (bottom panel). Energies are given in eV

The electron affinity is also very sensitive to cluster size. For  $N = 5$  (top panel of Fig. 8), the largest values of the VEA are found along Fe<sub>2</sub>, Fe<sub>3</sub>, and Fe<sub>4</sub> lines, reaching a maximum for Fe<sub>3</sub>Pd<sub>2</sub>. The binary configurations with the lowest values correspond to the CoPd edge, and also to the FePd<sub>4</sub> cluster. For  $N = 6$  (middle

panel of Fig. 8), the largest VEA correspond to Pd<sub>2</sub> or Pd<sub>3</sub>, regardless of the Fe and Co composition, particularly for Fe<sub>2</sub>CoPd<sub>3</sub>, Fe<sub>2</sub>Co<sub>2</sub>Pd<sub>2</sub>, FeCo<sub>3</sub>Pd<sub>2</sub>, and Co<sub>4</sub>Pd<sub>2</sub>. The lowest value is observed for CoPd<sub>5</sub>. Finally, for  $N = 7$  (bottom panel of Fig. 8), the largest VEA values are observed over the whole triangle (particularly for Fe<sub>2</sub>Pd<sub>5</sub>), excluding the FeCo binary edge and the Fe-rich corner.

### Magnetic moments

The magnetic behavior of the nanoalloys is illustrated in Fig. 9 for  $N = 5$ ,  $N = 6$ , and  $N = 7$ . In order to provide a clear picture of the magnetic moment dependence on composition we adopt a different representation than the Gibbs triangle used previously for the geometric and electronic properties.

When dealing with pristine nanoclusters, the total magnetic moment of pure Fe<sub>*x*</sub> clusters increases from  $18\mu_B$  for  $x = 5$  to  $22\mu_B$  for  $x = 7$ . Our results overestimate the experimental values for the spin contribution (Niemeyer et al. 2012). When compared with theoretical calculations, our results are in full agreement with the calculations results on Fe clusters of Guzmán-Ramírez et al. (2011, 2013), and compare reasonably well with other values reported (Yuan et al. 2013), although differences are found in some cases (see the work by of Rollmann et al. and references therein (Rollmann et al. 2006), where an extensive comparison of the different calculations is presented. In the same way, the total magnetic moment of pure Co clusters increases from  $13\mu_B$  for  $y = 5$  to  $15\mu_B$  for  $y = 7$ , in full agreement with the results of Guzmán-Ramírez et al. (2011, 2013). Moreover, our values are in the range of  $2.15$  to  $2.60\mu_B/\text{atom}$  in agreement with many of the theoretical values already reported (see the work of Rodríguez-López and references therein (Rodríguez-López et al. 2003). Finally, the total magnetic moment of pure Pd<sub>*z*</sub> clusters remains constant at  $2\mu_B$  for all values of  $z$ , in partial agreement with Barreateau et al. (2000) for  $N = 6$ .

It is interesting that the large Fe magnetic moment is always quenched very slowly and smoothly by the addition of Co. However, the addition of Pd tends to quench the total magnetic moment of Fe-rich and Co-rich structures in irregular steps, giving rise to a band-like behavior for all the sizes considered. This band-like behavior has been previously observed for

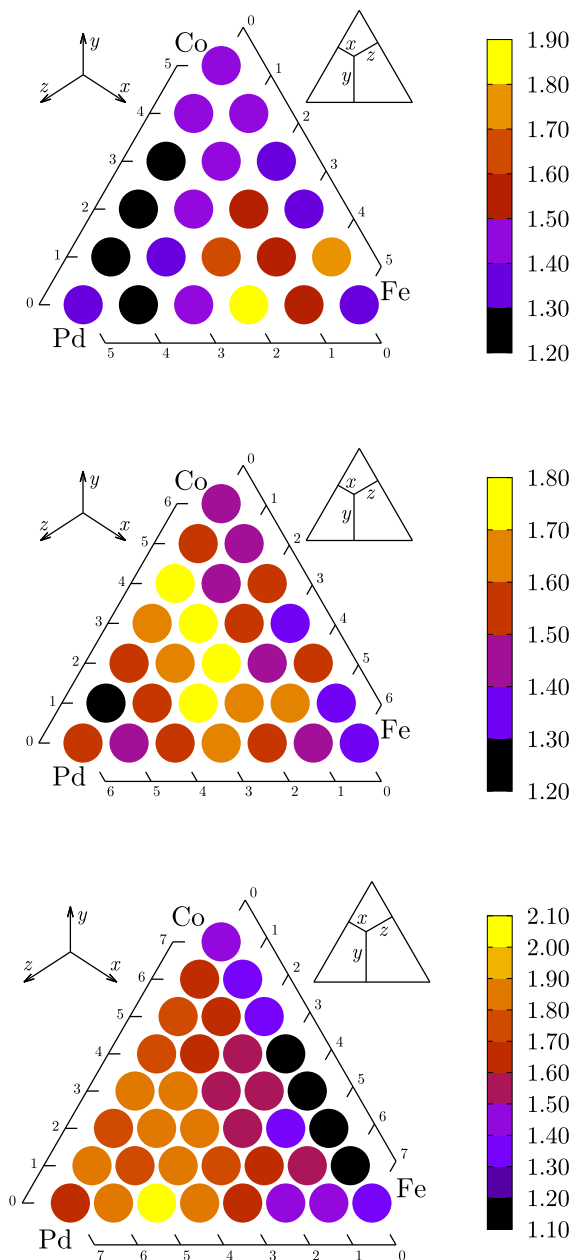


**Fig. 8** Vertical Electron Affinity (VEA) of the Fe<sub>*x*</sub>Co<sub>*y*</sub>Pd<sub>*z*</sub> nanoalloys, for  $x + y + z = 5$  (top panel),  $x + y + z = 6$  (center panel), and  $x + y + z = 7$  (bottom panel). Energies are given in eV

Fe<sub>*x*</sub>Co<sub>*y*</sub>Ni<sub>*z*</sub> ternary nanoclusters Varas et al. (2015), with  $x + y + z = 13$ .

In general, it is clear that a large and almost continuous range of magnetic moment values can be obtained by alloying. Therefore, transition metal

ternaries constitute a promising possibility for fine tuning nanocluster magnetic properties.

Although for very small clusters it is possible to guess the dependence of the magnetic moment as a function of composition, in terms of the atomic values, as the clusters size increases this becomes complicated due to the huge number of possible magnetic moment values, and the existence of degeneracies, as well as surface effects. However, it is possible to conjecture approximate expressions that hold in the Fe-, Co-, and Pd-rich concentration regions. In Fig. 9, it is also possible to observe band-like structures (close to the equiatomic regions) for the magnetic moments. This fact makes it difficult to guess a general expression that holds for all the concentration regions. However, for all the sizes, along the FeCo edge and in its vicinity, the local dependence of the magnetic moment can be written as follows:

$$\mu_T = (4x + 3y - C)\mu_B, \tag{7}$$

where  $C = 2$  for  $N = 5$ ,  $C = 4$  for  $N = 6$ , and  $C = 6$  for  $N = 7$ .

### Dissociation channels

We also examined and estimated the most likely dissociation channels for all the ternary clusters reported here. To do so, we calculate the lowest fragmentation energy  $E_f(N)$  required to break an  $N$  atom cluster into an  $N - M$  and an  $M$  one.  $E_f(N)$  is defined as

$$E_f(N) = E(N - M) + E(M) - E(N), \tag{8}$$

where  $E(N)$  is the total energy of the  $N$  atom cluster. When defined in this way  $E_f(N) > 0$ , which is useful to show that  $E_f(N)$  corresponds to the smallest fragmentation energy required to break an  $N$  atom cluster (Ur Rehman et al. 2011). However, some authors prefer to define it as  $E_f(N) = E(N) - E(N - M) - E(M) < 0$  Aguilera-Del-Toro et al. (2014). In Fig. 10, we present the lowest fragmentation energies of the clusters. They are always close to pure Pd clusters, and on the contrary, the largest values are always along the FeCo edge.

The most likely dissociation channels for the anionic structures are presented in Tables 2, 3, and 4 for  $N = 5, 6$ , and 7, respectively; for the cationic

structures in Tables 5, 6, and 7; and for the neutral structures in Tables 8, 9, and 10, respectively. All of these tables are to be found in Appendix.

In the numerical computation of the dissociation channels, we consider all the possible fragmentation paths, which means that we investigate not only single-atom fragmentation, but also molecular

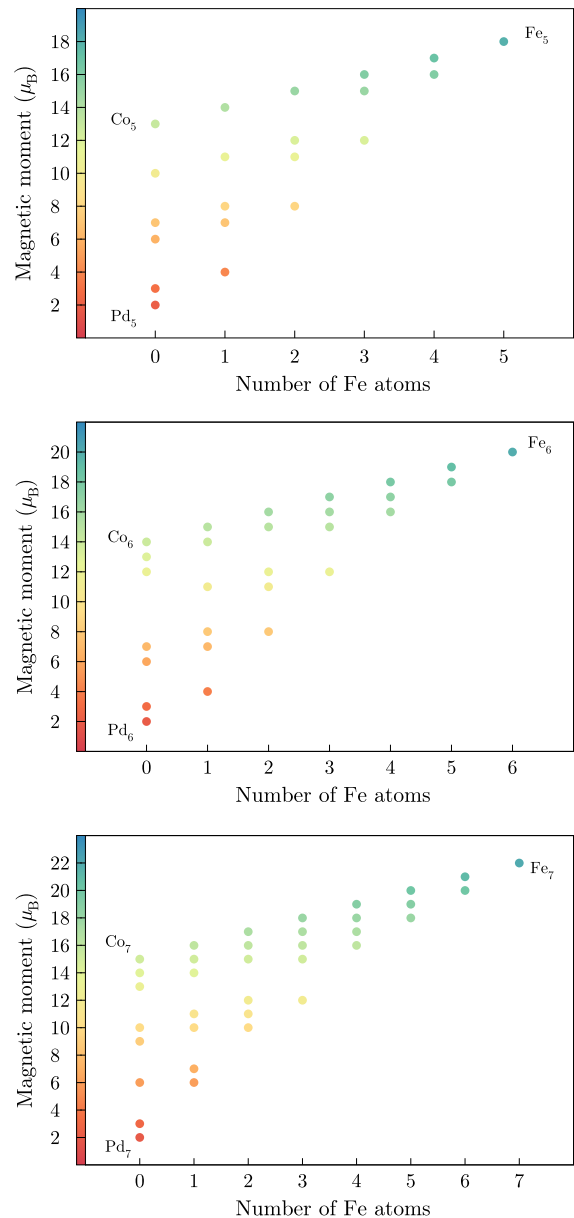


**Fig. 9** Total magnetic moment of the  $\text{Fe}_x\text{Co}_y\text{Pd}_z$  nanoalloys, for  $x + y + z = 5$  (top panel),  $x + y + z = 6$  (center panel), and  $x + y + z = 7$  (bottom panel)

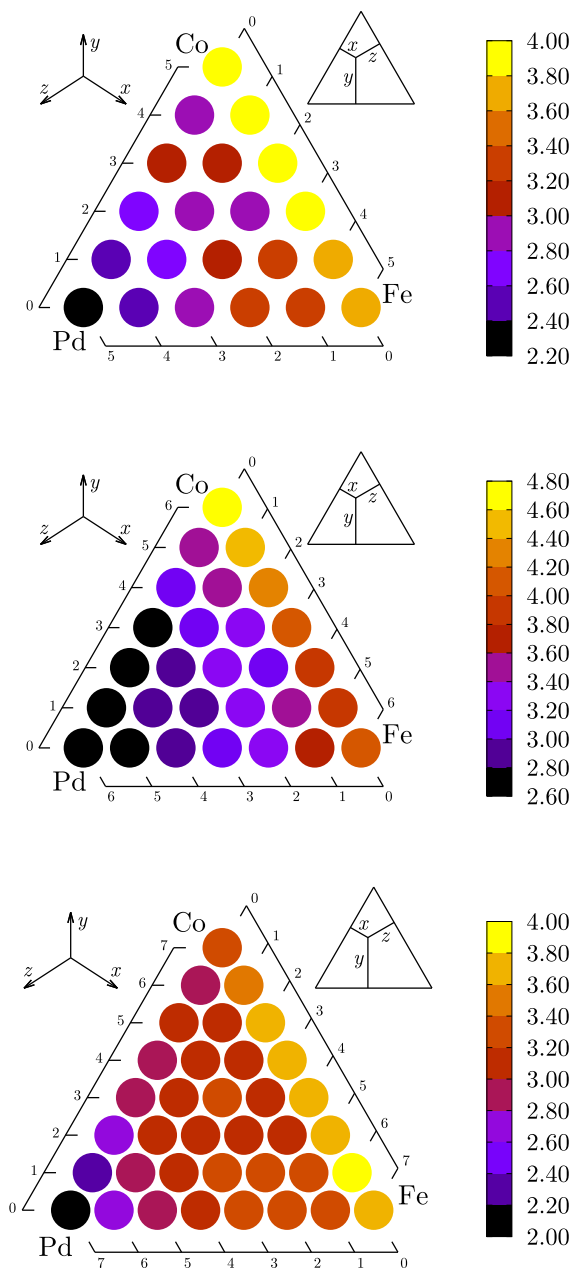


**Fig. 10** Lowest fragmentation energy of the  $\text{Fe}_x\text{Co}_y\text{Pd}_z$  nanoalloys, for  $x + y + z = 5$  (top panel),  $x + y + z = 6$  (center panel), and  $x + y + z = 7$  (bottom panel). Energies are in eV

breakup. Our results for the fragmentation channels of neutral, cationic, and anionic clusters indicate that the most likely path is through the atomic  $\text{Pd}^0$ ,  $\text{Pd}^+$ , and  $\text{Pd}^-$  channels when Pd is present. However, when Pd is absent, the most likely fragmentation channel is through the majority element. Molecular fragmentation channels are only observed for very small clusters,

in particular for  $\text{Co}_5^+$ ,  $\text{FeCo}_4^+$ ,  $\text{Fe}_2\text{Co}_3^+$ ,  $\text{Fe}_3\text{Co}_2^+$ ,  $\text{Fe}_4\text{Co}^+$ , and  $\text{Fe}_5^+$ . Some cases are also present for  $N = 4$  (see Supporting Information).

## Conclusions

An extensive calculation is reported of the minimal-energy geometries, the electronic, magnetic, and chemical properties, and the dissociation channels of  $N$  atom FeCoPd nanoclusters, for  $N \leq 7$ . We start finding all the geometrical local minima generated by a semiempirical Gupta potential search. Next, these structures are reoptimized using the SIESTA code to include the possibility of different total energy ordering of the many homotops and isomers.

Geometric and electronic properties of the ground state structure obtained by DFT optimization were computed. The geometric structures are similar to those reported for pure transition metal elements of the same size clusters; however, due to the multicomponent nature of the system, a huge variety of homotops and isomers are found.

For the interatomic distances, the results are as expected larger values are observed for the Pd-rich nanoalloys, and smaller ones in the Co-rich region. As far as the stability is concerned, the binding energy shows a monotonic dependence; the most stable structures are observed along the binary FeCo edge. In general, the largest tendency to mixing of the ternary system is observed for FePd binary systems and in their vicinity.

As far as the second energy difference is concerned, the most likely system to be generated in an experimental setup are FeCo binaries, and clusters with only a few Pd atoms. Segregation of this multicomponent system is observed near the vertices of the triangles (pure clusters), and mixing is observed at the center of the triangles, that is when the number of Fe, Co, and Pd atoms is similar. The ionization potential and electron affinity are very sensitive to the composition and cluster size.

The magnetic behavior displays a tiny variation as a function of composition, reflected in a very gradual color variation along the lines parallel to the main edges of the triangle (see Fig. 9). However, some discontinuities of the magnetic moment (or band-like behavior) are also observed.

Our results for the fragmentation channels indicate that a close correlation with the state of charge of the cluster does exist, and that the most likely fragmentation path is through atomic Pd<sup>0</sup>, Pd<sup>+</sup>, and Pd<sup>-</sup>, when Pd is present in the cluster. However, when Pd is absent, the most likely fragmentation channel is through the most abundant element in the cluster.

All in all, FeCoPd nanoclusters seem to be good candidates to tailor magnetic properties by tuning the cluster composition.

**Acknowledgments** This work was supported by the Fondo Nacional de Investigaciones Científicas y Tecnológicas (FONDECYT, Chile) under Grants #1160639 and 1130272 (MK and JR), and Financiamiento Basal para Centros Científicos y Tecnológicos de Excelencia-FB0807 (JR and MK). FAG acknowledges financial support from DIPC during an academic stay, and thanks Andres Vega and Carlos Balbás for helpful discussions, as well as D. Lasa from the DIPC computer center for his valuable help, and J. Limon for the support of the UASLP Computer Center.

**Appendix: Dissociation channels**

See Tables 2, 3, 4, 5, 6, 7, 8, 9, and 10.

**Table 2** Most favorable dissociation channels and corresponding dissociation energies  $E_f$  of  $Fe_xCo_yPd_z^-$  clusters, for  $x + y + z = 5$

$Fe_xCo_yPd_z^-$	Dissociation channel			$E_f$ (eV)
$Pd_5^-$	→	$Pd^-$	+ $Pd_4$	2.401
$CoPd_4^-$	→	$Pd^-$	+ $CoPd_3$	3.010
$Co_2Pd_3^-$	→	$Pd^-$	+ $Co_2Pd_2$	3.093
$Co_3Pd_2^-$	→	$Pd^-$	+ $Co_3Pd$	2.887
$Co_4Pd^-$	→	$Pd^-$	+ $Co_4$	3.198
$Co_5^-$	→	$Co^-$	+ $Co_4$	4.122
$FePd_4^-$	→	$Pd^-$	+ $FePd_3$	3.095
$FeCoPd_3^-$	→	$Pd^-$	+ $FeCoPd_2$	3.133
$FeCo_2Pd_2^-$	→	$Pd^-$	+ $FeCo_2Pd$	2.966
$FeCo_3Pd^-$	→	$Pd^-$	+ $FeCo_3$	3.143
$FeCo_4^-$	→	$Co^-$	+ $FeCo_3$	4.050
$Fe_2Pd_3^-$	→	$Pd^-$	+ $Fe_2Pd_2$	2.828
$Fe_2CoPd_2^-$	→	$Pd^-$	+ $Fe_2CoPd$	3.566
$Fe_2Co_2Pd^-$	→	$Pd^-$	+ $Fe_2Co_2$	3.267
$Fe_2Co_3^-$	→	$Co^-$	+ $FeCo_3$	3.989
$Fe_3Pd_2^-$	→	$Pd^-$	+ $Fe_3Pd$	3.779
$Fe_3CoPd^-$	→	$Pd^-$	+ $Fe_3Co$	3.128
$Fe_3Co_2^-$	→	$Fe^-$	+ $Fe_2Co_2$	4.056

**Table 2** continued

$Fe_xCo_yPd_z^-$	Dissociation channel			$E_f$ (eV)
$Fe_4Pd^-$	→	$Pd^-$	+ $Fe_4$	3.386
$Fe_4Co^-$	→	$Fe^-$	+ $Fe_3Co$	3.891
$Fe_5^-$	→	$Fe^-$	+ $Fe_4$	3.553

**Table 3** Most favorable dissociation channels and corresponding dissociation energies  $E_f$  of  $Fe_xCo_yPd_z^-$  clusters, for  $x + y + z = 6$

$Fe_xCo_yPd_z^-$	Dissociation channel			$E_f$ (eV)
$Pd_6^-$	→	$Pd^-$	+ $Pd_5$	2.930
$CoPd_5^-$	→	$Pd^-$	+ $CoPd_4$	2.609
$Co_2Pd_4^-$	→	$Pd^-$	+ $Co_2Pd_3$	2.913
$Co_3Pd_3^-$	→	$Pd^-$	+ $Co_3Pd_2$	3.107
$Co_4Pd_2^-$	→	$Pd^-$	+ $Co_4Pd$	3.515
$Co_5Pd^-$	→	$Pd^-$	+ $Co_5$	3.569
$Co_6^-$	→	$Co^-$	+ $Co_5$	4.651
$FePd_5^-$	→	$Pd^-$	+ $FePd_4$	2.702
$FeCoPd_4^-$	→	$Pd^-$	+ $FeCoPd_3$	3.045
$FeCo_2Pd_3^-$	→	$Pd^-$	+ $FeCo_2Pd_2$	3.082
$FeCo_3Pd_2^-$	→	$Pd^-$	+ $FeCo_3Pd$	3.352
$FeCo_4Pd^-$	→	$Pd^-$	+ $FeCo_4$	3.433
$FeCo_5^-$	→	$Co^-$	+ $FeCo_4$	4.472
$Fe_2Pd_4^-$	→	$Pd^-$	+ $Fe_2Pd_3$	3.117
$Fe_2CoPd_3^-$	→	$Pd^-$	+ $Fe_2CoPd_2$	3.014
$Fe_2Co_2Pd_2^-$	→	$Pd^-$	+ $Fe_2Co_2Pd$	3.440
$Fe_2Co_3Pd^-$	→	$Pd^-$	+ $Fe_2Co_3$	3.453
$Fe_2Co_4^-$	→	$Fe^-$	+ $FeCo_4$	4.439
$Fe_3Pd_3^-$	→	$Pd^-$	+ $Fe_3Pd_2$	2.892
$Fe_3CoPd_2^-$	→	$Pd^-$	+ $Fe_3CoPd$	3.358
$Fe_3Co_2Pd^-$	→	$Pd^-$	+ $Fe_3Co_2$	3.339
$Fe_3Co_3^-$	→	$Co^-$	+ $Fe_3Co_2$	4.204
$Fe_4Pd_2^-$	→	$Pd^-$	+ $Fe_4Pd$	3.449
$Fe_4CoPd^-$	→	$Pd^-$	+ $Fe_4Co$	3.413
$Fe_4Co_2^-$	→	$Co^-$	+ $Fe_4Co$	4.226
$Fe_5Pd^-$	→	$Pd^-$	+ $Fe_5$	3.767
$Fe_5Co^-$	→	$Fe^-$	+ $Fe_4Co$	3.600
$Fe_6^-$	→	$Fe^-$	+ $Fe_5$	4.158

**Table 4** Most favorable dissociation channels and corresponding dissociation energies  $E_f$  of  $Fe_xCo_yPd_z^-$  clusters, for  $x + y + z = 7$

$Fe_xCo_yPd_z^-$	Dissociation channel			$E_f$ (eV)
$Pd_7^-$	→	$Pd^-$	+ $Pd_6$	2.294
$CoPd_6^-$	→	$Pd^-$	+ $CoPd_5$	2.916



**Table 4** continued

$Fe_xCo_yPd_z^-$	Dissociation channel			$E_f$ (eV)
$Co_2Pd_5^-$	→	$Pd^-$	+ $Co_2Pd_4$	3.007
$Co_3Pd_4^-$	→	$Pd^-$	+ $Co_3Pd_3$	3.217
$Co_4Pd_3^-$	→	$Pd^-$	+ $Co_4Pd_2$	2.862
$Co_5Pd_2^-$	→	$Pd^-$	+ $Co_5Pd$	3.182
$Co_6Pd^-$	→	$Pd^-$	+ $Co_6$	3.173
$Co_7^-$	→	$Co^-$	+ $Co_6$	3.476
$FePd_6^-$	→	$Pd^-$	+ $FePd_5$	3.130
$FeCoPd_5^-$	→	$Pd^-$	+ $FeCoPd_4$	3.046
$FeCo_2Pd_4^-$	→	$Pd^-$	+ $FeCo_2Pd_3$	3.310
$FeCo_3Pd_3^-$	→	$Pd^-$	+ $FeCo_3Pd_2$	3.262
$FeCo_4Pd_2^-$	→	$Pd^-$	+ $FeCo_4Pd$	3.249
$FeCo_5Pd^-$	→	$Pd^-$	+ $FeCo_5$	3.251
$FeCo_6^-$	→	$Fe^-$	+ $Co_6$	3.464
$Fe_2Pd_5^-$	→	$Pd^-$	+ $Fe_2Pd_4$	3.364
$Fe_2CoPd_4^-$	→	$Pd^-$	+ $Fe_2CoPd_3$	3.263
$Fe_2Co_2Pd_3^-$	→	$Pd^-$	+ $Fe_2Co_2Pd_2$	3.250
$Fe_2Co_3Pd_2^-$	→	$Pd^-$	+ $Fe_2Co_3Pd$	3.231
$Fe_2Co_4Pd^-$	→	$Pd^-$	+ $Fe_2Co_4$	3.109
$Fe_2Co_5^-$	→	$Fe^-$	+ $Fe_1Co_5$	3.497
$Fe_3Pd_4^-$	→	$Pd^-$	+ $Fe_3Pd_3$	3.288
$Fe_3CoPd_3^-$	→	$Pd^-$	+ $Fe_3CoPd_2$	3.394
$Fe_3Co_2Pd_2^-$	→	$Pd^-$	+ $Fe_3Co_2Pd$	3.204
$Fe_3Co_3Pd^-$	→	$Pd^-$	+ $Fe_3Co_3$	3.223
$Fe_3Co_4^-$	→	$Fe^-$	+ $Fe_2Co_4$	3.415
$Fe_4Pd_3^-$	→	$Pd^-$	+ $Fe_4Pd_2$	3.331
$Fe_4CoPd_2^-$	→	$Pd^-$	+ $Fe_4CoPd$	3.266
$Fe_4Co_2Pd^-$	→	$Pd^-$	+ $Fe_4Co_2$	3.042
$Fe_4Co_3^-$	→	$Co^-$	+ $Fe_4Co_2$	3.693
$Fe_5Pd_2^-$	→	$Pd^-$	+ $Fe_5Pd$	3.338
$Fe_5CoPd^-$	→	$Pd^-$	+ $Fe_5Co$	3.479
$Fe_5Co_2^-$	→	$Fe^-$	+ $Fe_4Co_2Pd_0$	3.430
$Fe_6Pd^-$	→	$Pd^-$	+ $Fe_6$	3.389
$Fe_6Co^-$	→	$Fe^-$	+ $Fe_5Co$	3.745
$Fe_7^-$	→	$Fe^-$	+ $Fe_6$	3.803

**Table 5** Most favorable dissociation channels and corresponding dissociation energies  $E_f$  of  $Fe_xCo_yPd_z^+$  clusters, for  $x + y + z = 5$

$Fe_xCo_yPd_z^+$	Dissociation channel			$E_f$ (eV)
$Pd_5^+$	→	$Pd^+$	+ $Pd_4$	2.417
$CoPd_4^+$	→	$Pd^+$	+ $CoPd_3$	2.613
$Co_2Pd_3^+$	→	$Pd^+$	+ $Co_2Pd_2$	2.501
$Co_3Pd_2^+$	→	$Co^+$	+ $Co_2Pd_2$	3.199

**Table 5** continued

$Fe_xCo_yPd_z^+$	Dissociation channel			$E_f$ (eV)
$Co_4Pd^+$	→	$Pd^+$	+ $Co_4$	3.042
$Co_5^+$	→	$Co_2^+$	+ $Co_3$	3.465
$FePd_4^+$	→	$Pd^+$	+ $FePd_3$	2.701
$FeCoPd_3^+$	→	$Pd^+$	+ $FeCoPd_2$	2.641
$FeCo_2Pd_2^+$	→	$Co^+$	+ $FeCoPd_2$	3.218
$FeCo_3Pd^+$	→	$Pd^+$	+ $FeCo_3$	3.280
$FeCo_4^+$	→	$Co_2^+$	+ $FeCo_2$	3.636
$Fe_2Pd_3^+$	→	$Pd^+$	+ $Fe_2Pd_2$	3.090
$Fe_2CoPd_2^+$	→	$Pd^+$	+ $Fe_2CoPd$	3.180
$Fe_2Co_2Pd^+$	→	$Pd^+$	+ $Fe_2Co_2$	3.188
$Fe_2Co_3^+$	→	$FeCo^+$	+ $FeCo_2$	3.593
$Fe_3Pd_2^+$	→	$Pd^+$	+ $Fe_3Pd$	3.793
$Fe_3CoPd^+$	→	$Pd^+$	+ $Fe_3Co$	3.096
$Fe_3Co_2^+$	→	$FeCo^+$	+ $Fe_2Co$	3.590
$Fe_4Pd^+$	→	$Pd^+$	+ $Fe_4$	3.185
$Fe_4Co^+$	→	$FeCo^+$	+ $Fe_3$	3.607
$Fe_5^+$	→	$Fe_2^+$	+ $Fe_3$	3.751

**Table 6** Most favorable dissociation channels and corresponding dissociation energies  $E_f$  of  $Fe_xCo_yPd_z^+$  clusters, for  $x + y + z = 6$

$Fe_xCo_yPd_z^+$	Dissociation channel			$E_f$ (eV)
$Pd_6^+$	→	$Pd^+$	+ $Pd_5$	2.114
$CoPd_5^+$	→	$Pd^+$	+ $CoPd_4$	2.814
$Co_2Pd_4^+$	→	$Pd^+$	+ $Co_2Pd_3$	2.582
$Co_3Pd_3^+$	→	$Pd^+$	+ $Co_3Pd_2$	2.761
$Co_4Pd_2^+$	→	$Pd^+$	+ $Co_4Pd$	3.028
$Co_5Pd^+$	→	$Pd^+$	+ $Co_5$	3.408
$Co_6^+$	→	$Co^+$	+ $Co_5$	4.697
$FePd_5^+$	→	$Pd^+$	+ $FePd_4$	1.719
$FeCoPd_4^+$	→	$Pd^+$	+ $FeCoPd_3$	2.643
$FeCo_2Pd_3^+$	→	$Pd^+$	+ $FeCo_2Pd_2$	2.906
$FeCo_3Pd_2^+$	→	$Pd^+$	+ $FeCo_3Pd$	3.052
$FeCo_4Pd^+$	→	$Pd^+$	+ $FeCo_4$	3.242
$FeCo_5^+$	→	$Co^+$	+ $FeCo_4$	4.465
$Fe_2Pd_4^+$	→	$Pd^+$	+ $Fe_2Pd_3$	2.797
$Fe_2CoPd_3^+$	→	$Pd^+$	+ $Fe_2CoPd_2$	2.924
$Fe_2Co_2Pd_2^+$	→	$Pd^+$	+ $Fe_2Co_2Pd$	3.201
$Fe_2Co_3Pd^+$	→	$Pd^+$	+ $Fe_2Co_3$	3.190
$Fe_2Co_4^+$	→	$Co^+$	+ $Fe_2Co_3$	4.438
$Fe_3Pd_3^+$	→	$Pd^+$	+ $Fe_3Pd_2$	2.891
$Fe_3CoPd_2^+$	→	$Pd^+$	+ $Fe_3CoPd$	3.111

**Table 6** continued

$Fe_xCo_yPd_z^+$	Dissociation channel			$E_f$ (eV)
$Fe_3Co_2Pd^+$	→	$Pd^+$	+ $Fe_3Co_2$	3.331
$Fe_3Co_3^+$	→	$Co^+$	+ $Fe_3Co_2$	4.406
$Fe_4Pd_2^+$	→	$Pd^+$	+ $Fe_4Pd$	3.414
$Fe_4CoPd^+$	→	$Pd^+$	+ $Fe_4Co$	3.565
$Fe_4Co_2^+$	→	$Fe^+$	+ $Fe_3Co_2$	4.244
$Fe_5Pd^+$	→	$Pd^+$	+ $Fe_5$	3.399
$Fe_5Co^+$	→	$Fe^+$	+ $Fe_4Co$	4.125
$Fe_6^+$	→	$Fe^+$	+ $Fe_5$	4.193

**Table 7** Most favorable dissociation channels and corresponding dissociation energies  $E_f$  of  $Fe_xCo_yPd_z^+$  clusters, for  $x + y + z = 7$

$Fe_xCo_yPd_z^+$	Dissociation channel			$E_f$ (eV)
$Pd_7^+$	→	$Pd^+$	+ $Pd_6$	2.944
$CoPd_6^+$	→	$Pd^+$	+ $CoPd_5$	2.407
$Co_2Pd_5^+$	→	$Pd^+$	+ $Co_2Pd_4$	2.860
$Co_3Pd_4^+$	→	$Pd^+$	+ $Co_3Pd_3$	2.893
$Co_4Pd_3^+$	→	$Pd^+$	+ $Co_4Pd_2$	3.120
$Co_5Pd_2^+$	→	$Pd^+$	+ $Co_5Pd$	3.202
$Co_6Pd^+$	→	$Pd^+$	+ $Co_6$	3.077
$Co_7^+$	→	$Co^+$	+ $Co_6$	4.010
$FePd_6^+$	→	$Pd^+$	+ $FePd_5$	3.478
$FeCoPd_5^+$	→	$Pd^+$	+ $FeCoPd_4$	2.921
$FeCo_2Pd_4^+$	→	$Pd^+$	+ $FeCo_2Pd_3$	2.830
$FeCo_3Pd_3^+$	→	$Pd^+$	+ $FeCo_3Pd_2$	3.120
$FeCo_4Pd_2^+$	→	$Pd^+$	+ $FeCo_4Pd$	3.222
$FeCo_5Pd^+$	→	$Pd^+$	+ $FeCo_5$	3.095
$FeCo_6^+$	→	$Co^+$	+ $FeCo_5$	4.005
$Fe_2Pd_5^+$	→	$Pd^+$	+ $Fe_2Pd_4$	2.869
$Fe_2CoPd_4^+$	→	$Pd^+$	+ $Fe_2CoPd_3$	2.910
$Fe_2Co_2Pd_3^+$	→	$Pd^+$	+ $Fe_2Co_2Pd_2$	3.146
$Fe_2Co_3Pd_2^+$	→	$Pd^+$	+ $Fe_2Co_3Pd$	3.364
$Fe_2Co_4Pd^+$	→	$Pd^+$	+ $Fe_2Co_4$	3.181
$Fe_2Co_5^+$	→	$Co^+$	+ $Fe_2Co_4$	4.014
$Fe_3Pd_4^+$	→	$Pd^+$	+ $Fe_3Pd_3$	2.939
$Fe_3CoPd_3^+$	→	$Pd^+$	+ $Fe_3CoPd_2$	3.435
$Fe_3Co_2Pd_2^+$	→	$Pd^+$	+ $Fe_3Co_2Pd$	3.194
$Fe_3Co_3Pd^+$	→	$Pd^+$	+ $Fe_3Co_3$	3.148
$Fe_3Co_4^+$	→	$Co^+$	+ $Fe_3Co_3$	4.223
$Fe_4Pd_3^+$	→	$Pd^+$	+ $Fe_4Pd_2$	3.341
$Fe_4CoPd_2^+$	→	$Pd^+$	+ $Fe_4CoPd$	3.076
$Fe_4Co_2Pd^+$	→	$Pd^+$	+ $Fe_4Co_2$	3.072
$Fe_4Co_3^+$	→	$Co^+$	+ $Fe_4Co_2$	4.199

**Table 7** continued

$Fe_xCo_yPd_z^+$	Dissociation channel			$E_f$ (eV)
$Fe_5Pd_2^+$	→	$Pd^+$	+ $Fe_5Pd$	3.593
$Fe_5CoPd^+$	→	$Pd^+$	+ $Fe_5Co$	3.340
$Fe_5Co_2^+$	→	$Fe^+$	+ $Fe_4Co_2$	3.974
$Fe_6Pd^+$	→	$Pd^+$	+ $Fe_6$	3.198
$Fe_6Co^+$	→	$Fe^+$	+ $Fe_5Co$	4.123
$Fe_7^+$	→	$Fe^+$	+ $Fe_6$	3.891

**Table 8** Most favorable dissociation channels and corresponding dissociation energies  $E_f$  of  $Fe_xCo_yPd_z$  neutral clusters, for  $x + y + z = 5$

$Fe_xCo_yPd_z$	Dissociation channel			$E_f$ (eV)
$Pd_5$	→	$Pd$	+ $Pd_4$	2.302
$CoPd_4$	→	$Pd$	+ $CoPd_3$	2.416
$Co_2Pd_3$	→	$Pd$	+ $Co_2Pd_2$	2.739
$Co_3Pd_2$	→	$Pd$	+ $Co_3Pd$	3.064
$Co_4Pd$	→	$Pd$	+ $Co_4$	2.879
$Co_5$	→	$Co$	+ $Co_4$	3.822
$FePd_4$	→	$Pd$	+ $FePd_3$	2.568
$FeCoPd_3$	→	$Pd$	+ $FeCoPd_2$	2.749
$FeCo_2Pd_2$	→	$Pd$	+ $FeCo_2Pd$	2.927
$FeCo_3Pd$	→	$Pd$	+ $FeCo_3$	3.063
$FeCo_4$	→	$Fe$	+ $FeCo_3$	3.957
$Fe_2Pd_3$	→	$Pd$	+ $Fe_2Pd_2$	2.828
$Fe_2CoPd_2$	→	$Pd$	+ $Fe_2CoPd$	3.127
$Fe_2Co_2Pd$	→	$Pd$	+ $Fe_2Co_2$	2.964
$Fe_2Co_3$	→	$Co$	+ $Fe_2Co_2$	3.955
$Fe_3Pd_2$	→	$Pd$	+ $Fe_3Pd$	3.373
$Fe_3CoPd$	→	$Pd$	+ $Fe_3Co$	3.233
$Fe_3Co_2$	→	$Fe$	+ $Fe_2Co_2$	3.979
$Fe_4Pd$	→	$Pd$	+ $Fe_4$	3.331
$Fe_4Co$	→	$Fe$	+ $Fe_3Co$	3.795
$Fe_5$	→	$Fe$	+ $Fe_4$	3.679

**Table 9** Most favorable dissociation channels and corresponding dissociation energies  $E_f$  of  $Fe_xCo_yPd_z$  neutral clusters, for  $x + y + z = 6$

$Fe_xCo_yPd_z$	Dissociation channel			$E_f$ (eV)
$Pd_6$	→	$Pd$	+ $Pd_5$	2.665
$CoPd_5$	→	$Pd$	+ $CoPd_4$	2.625
$Co_2Pd_4$	→	$Pd$	+ $Co_2Pd_3$	2.654
$Co_3Pd_3$	→	$Pd$	+ $Co_3Pd_2$	2.705
$Co_4Pd_2$	→	$Pd$	+ $Co_4Pd$	3.174

**Table 9** continued

$\text{Fe}_x\text{Co}_y\text{Pd}_z$	Dissociation channel			$E_f$ (eV)
$\text{Co}_5\text{Pd}$	→	Pd	+ $\text{Co}_5$	3.430
$\text{Co}_6$	→	Co	+ $\text{Co}_5$	4.647
$\text{FePd}_5$	→	Pd	+ $\text{FePd}_4$	2.601
$\text{FeCoPd}_4$	→	Pd	+ $\text{FeCoPd}_3$	2.858
$\text{FeCo}_2\text{Pd}_3$	→	Pd	+ $\text{FeCo}_2\text{Pd}_2$	2.887
$\text{FeCo}_3\text{Pd}_2$	→	Pd	+ $\text{FeCo}_3\text{Pd}$	3.094
$\text{FeCo}_4\text{Pd}$	→	Pd	+ $\text{FeCo}_4$	3.430
$\text{FeCo}_5$	→	Co	+ $\text{FeCo}_4$	4.487
$\text{Fe}_2\text{Pd}_4$	→	Pd	+ $\text{Fe}_2\text{Pd}_3$	2.979
$\text{Fe}_2\text{CoPd}_3$	→	Pd	+ $\text{Fe}_2\text{CoPd}_2$	2.931
$\text{Fe}_2\text{Co}_2\text{Pd}_2$	→	Pd	+ $\text{Fe}_2\text{Co}_2\text{Pd}$	3.231
$\text{Fe}_2\text{Co}_3\text{Pd}$	→	Pd	+ $\text{Fe}_2\text{Co}_3$	3.241
$\text{Fe}_2\text{Co}_4$	→	Co	+ $\text{Fe}_2\text{Co}_3$	4.313
$\text{Fe}_3\text{Pd}_3$	→	Pd	+ $\text{Fe}_3\text{Pd}_2$	3.019
$\text{Fe}_3\text{CoPd}_2$	→	Pd	+ $\text{Fe}_3\text{CoPd}$	3.255
$\text{Fe}_3\text{Co}_2\text{Pd}$	→	Pd	+ $\text{Fe}_3\text{Co}_2$	3.147
$\text{Fe}_3\text{Co}_3$	→	Co	+ $\text{Fe}_3\text{Co}_2$	4.151
$\text{Fe}_4\text{Pd}_2$	→	Pd	+ $\text{Fe}_4\text{Pd}$	3.396
$\text{Fe}_4\text{CoPd}$	→	Pd	+ $\text{Fe}_4\text{Co}$	3.487
$\text{Fe}_4\text{Co}_2$	→	Fe	+ $\text{Fe}_3\text{Co}_2$	3.805
$\text{Fe}_5\text{Pd}$	→	Pd	+ $\text{Fe}_5$	3.653
$\text{Fe}_5\text{Co}$	→	Fe	+ $\text{Fe}_4\text{Co}$	3.974
$\text{Fe}_6$	→	Fe	+ $\text{Fe}_5$	4.171

**Table 10** Most favorable dissociation channels and corresponding dissociation energies  $E_f$  of  $\text{Fe}_x\text{Co}_y\text{Pd}_z$  neutral clusters, for  $x + y + z = 7$ 

$\text{Fe}_x\text{Co}_y\text{Pd}_z$	Dissociation channel			$E_f$ (eV)
$\text{Pd}_7$	→	Pd	+ $\text{Pd}_6$	2.174
$\text{CoPd}_6$	→	Pd	+ $\text{CoPd}_5$	2.345
$\text{Co}_2\text{Pd}_5$	→	Pd	+ $\text{Co}_2\text{Pd}_4$	2.783
$\text{Co}_3\text{Pd}_4$	→	Pd	+ $\text{Co}_3\text{Pd}_3$	2.992
$\text{Co}_4\text{Pd}_3$	→	Pd	+ $\text{Co}_4\text{Pd}_2$	2.923
$\text{Co}_5\text{Pd}_2$	→	Pd	+ $\text{Co}_5\text{Pd}$	3.006
$\text{Co}_6\text{Pd}$	→	Pd	+ $\text{Co}_6$	2.984
$\text{Co}_7$	→	Co	+ $\text{Co}_6$	3.391
$\text{FePd}_6$	→	Pd	+ $\text{FePd}_5$	2.730
$\text{FeCoPd}_5$	→	Pd	+ $\text{FeCoPd}_4$	2.810
$\text{FeCo}_2\text{Pd}_4$	→	Pd	+ $\text{FeCo}_2\text{Pd}_3$	3.092
$\text{FeCo}_3\text{Pd}_3$	→	Pd	+ $\text{FeCo}_3\text{Pd}_2$	3.119
$\text{FeCo}_4\text{Pd}_2$	→	Pd	+ $\text{FeCo}_4\text{Pd}$	3.061
$\text{FeCo}_5\text{Pd}$	→	Pd	+ $\text{FeCo}_5$	3.044
$\text{FeCo}_6$	→	Fe	+ $\text{Co}_6$	3.483

**Table 10** continued

$\text{Fe}_x\text{Co}_y\text{Pd}_z$	Dissociation channel			$E_f$ (eV)
$\text{Fe}_2\text{Pd}_5$	→	Pd	+ $\text{Fe}_2\text{Pd}_4$	2.911
$\text{Fe}_2\text{CoPd}_4$	→	Pd	+ $\text{Fe}_2\text{CoPd}_3$	3.187
$\text{Fe}_2\text{Co}_2\text{Pd}_3$	→	Pd	+ $\text{Fe}_2\text{Co}_2\text{Pd}_2$	3.100
$\text{Fe}_2\text{Co}_3\text{Pd}_2$	→	Pd	+ $\text{Fe}_2\text{Co}_3\text{Pd}$	3.202
$\text{Fe}_2\text{Co}_4\text{Pd}$	→	Pd	+ $\text{Fe}_2\text{Co}_4$	3.102
$\text{Fe}_2\text{Co}_5$	→	Co	+ $\text{Fe}_2\text{Co}_4$	3.660
$\text{Fe}_3\text{Pd}_4$	→	Pd	+ $\text{Fe}_3\text{Pd}_3$	3.098
$\text{Fe}_3\text{CoPd}_3$	→	Pd	+ $\text{Fe}_3\text{CoPd}_2$	3.221
$\text{Fe}_3\text{Co}_2\text{Pd}_2$	→	Pd	+ $\text{Fe}_3\text{Co}_2\text{Pd}$	3.193
$\text{Fe}_3\text{Co}_3\text{Pd}$	→	Pd	+ $\text{Fe}_3\text{Co}_3$	3.078
$\text{Fe}_3\text{Co}_4\text{Pd}$	→	Fe	+ $\text{Fe}_2\text{Co}_4$	3.721
$\text{Fe}_4\text{Pd}_3$	→	Pd	+ $\text{Fe}_4\text{Pd}_2$	3.253
$\text{Fe}_4\text{CoPd}_2$	→	Pd	+ $\text{Fe}_4\text{CoPd}$	3.263
$\text{Fe}_4\text{Co}_2\text{Pd}$	→	Pd	+ $\text{Fe}_4\text{Co}_2$	3.187
$\text{Fe}_4\text{Co}_3$	→	Fe	+ $\text{Fe}_3\text{Co}_3$	3.713
$\text{Fe}_5\text{Pd}_2$	→	Pd	+ $\text{Fe}_5\text{Pd}$	3.301
$\text{Fe}_5\text{CoPd}$	→	Pd	+ $\text{Fe}_5\text{Co}$	3.309
$\text{Fe}_5\text{Co}_2$	→	Fe	+ $\text{Fe}_4\text{Co}_2$	3.778
$\text{Fe}_6\text{Pd}$	→	Pd	+ $\text{Fe}_6$	3.268
$\text{Fe}_6\text{Co}$	→	Fe	+ $\text{Fe}_5\text{Co}$	3.936
$\text{Fe}_7$	→	Fe	+ $\text{Fe}_6$	3.794

## References

- Aguilera-Del-Toro RH, Aguilera-Granja F, Vega A, Balbás LC (2014) Structure, fragmentation patterns, and magnetic properties of small cobalt oxide clusters. *Phys Chem Chem Phys* 16(39):21732–21741. doi:10.1039/c4cp03370a, <http://dx.doi.org/10.1039/C4CP03370A>
- Aguilera-Granja F, García-Fuente A, Vega A (2008) Comparative *ab initio* study of the structural, electronic, and magnetic trends of isoelectronic late 3d and 4d transition metal clusters. *Phys Rev B* 78:134,425. doi:10.1103/PhysRevB.78.134425, <http://link.aps.org/doi/10.1103/PhysRevB.78.134425>
- Aguilera-Granja F, Piotrowski MJ, da Silva JL (2013) Structural and electronic properties of  $\text{TM}_{23-p}\text{Ag}_p$  (TM = Ni, Pd, and Pt) clusters in the dilute limit ( $p = 0-4$ ): a density functional theory investigation. *Eur Phys J D* 67(2):1–7. doi:10.1140/epjd/e2012-30447-y, <http://dx.doi.org/10.1140/epjd/e2012-30447-y>
- Barreteau C, Guirado-López R, Spanjaard D, Desjonquères MC, Oleś AM (2000) spd tight-binding model of magnetism in transition metals: Application to Rh and Pd clusters and slabs. *Phys Rev B* 61(11):7781–7794. doi:10.1103/PhysRevB.61.7781, <http://link.aps.org/doi/10.1103/PhysRevB.61.7781>

- Billas IML, Châtelain A, de Heer W (1994) Magnetism from the Atom to the Bulk in Iron, Cobalt, and Nickel Clusters. *Science* 265:1682. doi:10.1126/science.265.5179.1682, <http://science.sciencemag.org/content/265/5179/1682>
- Bonačić-Koutecký V, Fantucci P, Koutecký J (1991) Quantum chemistry of small clusters of elements of groups Ia, Ib, and IIa: fundamental concepts, predictions, and interpretation of experiments. *Chem Rev* 91:1035. doi:10.1021/cr00005a016
- Cantera-López H, Montejano-Carrizales JM, Aguilera-Granja F, Morán-López JL (2010) Theoretical study of bimetallic magnetic nanostructures:  $\text{Co}_n\text{Pd}_{N-n}$ ,  $n = 0, 1, \dots, N$ ,  $N = 3, 5, 7, 13$ . *Eur Phys J D* 57(1):61–69. doi:10.1140/epjd/e2010-00018-7, <http://www.springerlink.com/index/10.1140/epjd/e2010-00018-7>
- Castleman AW (2011) From Elements to Clusters: The Periodic Table Revisited. *J Phys Chem Lett* 2:1062–1069. doi:10.1021/jz200215s
- Cleri F, Rosato V (1993) Tight-binding potentials for transition metals and alloys. *Phys Rev B* 48:22–33. doi:10.1103/PhysRevB.48.22, <http://link.aps.org/doi/10.1103/PhysRevB.48.22>
- Ducastelle F (1991) In: de Boer FR, Petifor DG (eds) *Order and Phase Stability in Alloys*. North-Holland, Amsterdam
- Fallah V, Ofori-Opoku N, Stolle J, Provatas N, Esmaili S (2013) Simulation of early-stage clustering in ternary metal alloys using the phase-field crystal method. *Acta Mater* 61(10):3653–3666. doi:10.1016/j.actamat.2013.02.053
- Ferrando R, Jellinek J, Johnston RL (2008) Nanoalloys: From Theory to Applications of Alloy Clusters and Nanoparticles. *Chem Rev* 108(3):845–910. doi:10.1021/cr040090g, <http://dx.doi.org/10.1021/cr040090g>, and references therein
- Guillopé M, Legrand B (1989) (110) Surface stability in noble metals. *Surf Sci* 215(3):577–595. doi:10.1016/0039-6028(89)90277-X, <http://www.sciencedirect.com/science/article/pii/003960288990277X>
- Gupta RP (1981) Lattice relaxation at a metal surface. *Phys Rev B* 23:6265–6270. doi:10.1103/PhysRevB.23.6265, <http://link.aps.org/doi/10.1103/PhysRevB.23.6265>
- Guzmán-Ramírez G, Robles J, Vega A, Aguilera-Granja F (2011) Stability, structural, and magnetic phase diagrams of ternary ferromagnetic 3d-transition-metal clusters with five and six atoms. *J Chem Phys* 134(5):054101. doi:10.1063/1.3533954, <http://scitation.aip.org/content/aip/journal/jcp/134/5/10.1063/1.3533954>
- Guzmán-Ramírez G, Salvador P, Robles J, Vega A, Aguilera-Granja F (2013) Density functional study of ternary  $\text{Fe}_x\text{Co}_y\text{Ni}_z$  ( $x + y + z = 7$ ) clusters. *Theor Chem Acc* 132:1318. doi:10.1007/s00214-012-1318-4, <http://dx.doi.org/10.1007/s00214-012-1318-4>
- Kittel C (1996) *Introduction to Solid State Physics*, 7th edn. Wiley, New York
- Kleinman L, Bylander DM (1982) Efficacious Form for Model Pseudopotentials. *Phys Rev Lett* 48:1425–1428. doi:10.1103/PhysRevLett.48.1425, <http://link.aps.org/doi/10.1103/PhysRevLett.48.1425>
- Knickerbein MB (2001) Experimental Observation of Superparamagnetism in Manganese Clusters. *Phys Rev Lett* 86:5255–5257. doi:10.1103/PhysRevLett.86.5255, <http://link.aps.org/doi/10.1103/PhysRevLett.86.5255>
- Lee J, Scheraga H, Rackovsky S (1997) New optimization method for conformational energy calculations on polypeptides: conformational space annealing. *J Comput Chem* 18:1222. doi:10.1002/(SICI)1096-987X(19970715)18:9<1222::AID-JCC10>3.0.CO;2-7
- Lee J, Lee IH, Lee J (2003) Unbiased global optimization of Lennard-Jones clusters for  $N \leq 201$  using the conformational space annealing method. *Phys Rev Lett* 91(080):201. doi:10.1103/PhysRevLett.91.080201
- Ma L, Wang J, Hao Y, Wang G (2013) Density functional theory study of  $\text{FePd}_n$  ( $n = 2-14$ ) clusters and interactions with small molecules. *Comput Mater Sci* 68:166–173. doi:10.1016/j.commatsci.2012.10.014, <http://www.sciencedirect.com/science/article/pii/S0927025612006155>
- Martienssen W, Warlimont H (eds) (2005) *Springer Handbook of Condensed Matter and Materials Data*, 1st edn. Springer, Berlin
- Martínez-Herrera FJ, Mejía-Lira F, Aguilera-Granja F, Morán-López JL (1985) Theory of phase equilibria in Co-Fe alloys. *Phys Rev B* 31:1686–1688. doi:10.1103/PhysRevB.31.1686, <http://link.aps.org/doi/10.1103/PhysRevB.31.1686>
- Massalski TB, Okamoto H, Subramanian PK, Kacprzak L (eds) (1990) *Binary Alloy Phase Diagrams*, 2nd edn. American Society for Metals Park, OH
- Miralrio A, Sansores LE (2014) Electronic structure and stability of binary and ternary aluminum-bismuth-nitrogen nanoclusters. *Int J Quantum Chem*. doi:10.1002/qua.24693, <http://dx.doi.org/10.1002/qua.24693>
- Mokkath JH (2014) Magnetism, structure and chemical order in small CoPd clusters: a first-principles study. *J Magn Magn Mater* 349:109–115. doi:10.1016/j.jmmm.2013.08.050, <http://www.sciencedirect.com/science/article/pii/S030488531300615X>
- Montejano-Carrizales J, Aguilera-Granja F, Morán-López J (2011) Structural and magnetic properties of  $\text{Fe}_m\text{Y}_n$  ( $m + n = 7$ ,  $Y = \text{Ru, Rh, Pd, and Pt}$ ) nanoalloys. *Eur Phys J D* 64(1):53–62. doi:10.1140/epjd/e2011-20178-0, <http://www.springerlink.com/index/10.1140/epjd/e2011-20178-0>
- Muñoz F, Rogan J, Valdivia J, Varas A, Kiwi M (2013a) Binary cluster collision dynamics and minimum energy conformations. *Phys B: Condens Matter* 427:76–84. doi:10.1016/j.physb.2013.06.036, <http://www.sciencedirect.com/science/article/pii/S0921452613004092>
- Munoz F, Varas A, Rogan J, Valdivia JA, Kiwi M (2015)  $\text{Au}_{13-n}\text{Ag}_n$  clusters: a remarkably simple trend. *Phys. Chem. Chem. Phys.* 17(45):30492–30498. doi:10.1039/c5cp05664k, <http://pubs.rsc.org/en/content/articlehtml/2015/cp/c5cp05664k>
- Muñoz M, Varas A, Cárdenas C, Rogan J, Fuentealba P (2013b) Performance of modified Lennard-Jones potential to seed *ab initio* calculations of small cadmium clusters. *Comput Theor Chem* 1021:249–255. doi:10.1016/j.comptc.2013.07.041, <http://www.sciencedirect.com/science/article/pii/S2210271X13003289>, clusters: From Dimers to Nanoparticles
- Niemeyer M, Hirsch K, Zamudio-Bayer V, Langenberg A, Vogel M, Kossick M, Ebrecht C, Egashira K, Terasaki A, Möller T, Issendorff BV, Lau JT (2012) Spin Coupling and Orbital Angular Momentum Quenching in Free Iron Clusters. *Phys Rev Lett* 108(5):057201. doi:10.1103/PhysRevLett.108.057201, <http://journals.aps.org/prl/abstract/10.1103/PhysRevLett.108.057201>

- Perdew JP, Burke K, Ernzerhof M (1996) Generalized Gradient Approximation Made Simple. *Phys Rev Lett* 77:3865–3868. doi:10.1103/PhysRevLett.77.3865, <http://link.aps.org/doi/10.1103/PhysRevLett.77.3865>
- Petzow G, Effenberg G (eds) (1989) Ternary alloys: A comprehensive compendium of evaluated constitutional data and phase diagrams. VCH Verlagsgesellschaft, Weinheim
- Polak M, Rubinovich L (2005) Prediction of intercluster separation and Schottky-type heat-capacity contribution in surface-segregated binary and ternary alloy nanocluster systems. *Phys Rev B* 71:125426. doi:10.1103/PhysRevB.71.125426, <http://link.aps.org/doi/10.1103/PhysRevB.71.125426>
- Press WH, Teukolsky SA, Vetterling WT, Flannery BP (1992) Numerical Recipes in Fortran, 2nd edn. Cambridge University Press, Cambridge
- Rodríguez-López J, Aguilera-Granja F, Michaelian K, Vega A (2003) Structure and magnetism of cobalt clusters. *Phys Rev B* 67(17):1–9. doi:10.1103/PhysRevB.67.174413, <http://link.aps.org/doi/10.1103/PhysRevB.67.174413>
- Rogan J, García G, Loyola C, Orellana W, Ramírez R, Kiwi M (2006) Alternative search strategy for minimal energy nanocluster structures: the case of rhodium, palladium and silver. *J Chem Phys* 125(214):708. doi:10.1063/1.2402168
- Rogan J, Ramírez M, Varas A, Kiwi M (2013a) How relevant is the choice of classical potentials in finding minimal energy cluster conformations? *Comput Theor Chem* 1021:155–163. <http://dx.doi.org/10.1016/j.comptc.2013.07.004>, <http://www.sciencedirect.com/science/article/pii/S2210271X13002843>, clusters: From Dimers to Nanoparticles
- Rogan J, Varas A, Valdivia JA, Kiwi M (2013b) A strategy to find minimal energy nanocluster structures. *J Comput Chem* 34(29):2548–2556. doi:10.1002/jcc.23419, <http://dx.doi.org/10.1002/jcc.23419>
- Rollmann G, Entel P, Sahoo S (2006) Competing structural and magnetic effects in small iron clusters. *Comput Mater Sci* 35(3):275–278. doi:10.1016/j.commatsci.2004.09.059, <http://www.sciencedirect.com/science/article/pii/S0927025605001369>
- Rubinovich L, Polak M (2004) Site-specific segregation and compositional ordering in Ni-based ternary alloy nanoclusters computed by the free-energy concentration expansion method. *Phys Rev B* 69:155405. doi:10.1103/PhysRevB.69.155405, <http://link.aps.org/doi/10.1103/PhysRevB.69.155405>
- Soler JM, Artacho E, Gale JD, García A, Junquera J, Ordejón P, Sánchez-Portal D (2002) The SIESTA method for *ab initio* order-*N* materials simulation. *J Phys Condens Matter* 14(11):2745. <http://stacks.iop.org/0953-8984/14/i=11/a=302>
- Sourmail T (2005) Near equiatomic FeCo alloys: constitution, mechanical and magnetic properties. *Prog Mater Sci* 50(7):816–880. doi:10.1016/j.pmatsci.2005.04.001, <http://www.sciencedirect.com/science/article/pii/S007964250500204>
- Sun S, Murray CB, Weller D, Folks L, Moser A (2000) Monodisperse FePt Nanoparticles and Ferromagnetic FePt Nanocrystal Superlattices. *Science* 287:1989. doi:10.1126/science.287.5460.1989, <http://science.sciencemag.org/content/287/5460/1989>
- Troullier N, Martins JL (1991) Efficient pseudopotentials for plane-wave calculations. *Phys Rev B* 43:1993–2006. doi:10.1103/PhysRevB.43.1993, <http://link.aps.org/doi/10.1103/PhysRevB.43.1993>
- Ur Rehman H, Springborg M, Dong Y (2011) Structural and Electronic Properties of  $\text{Si}_n$ ,  $\text{Ge}_n$ , and  $\text{Si}_n\text{Ge}_n$  clusters. *J Phys Chem A* 115(10):2005–2015. doi:10.1021/jp109198r, <http://dx.doi.org/10.1021/jp109198r>
- Varas A, Aguilera-Granja F, Rogan J, Kiwi M (2015) Structural, electronic, and magnetic properties of  $\text{Fe}_x\text{Co}_y\text{Ni}_z$  ( $x + y + z = 13$ ) clusters: A density-functional-theory study. *J Magn Magn Mater* 394:325–334. doi:10.1016/j.jmmm.2015.06.088, <http://www.sciencedirect.com/science/article/pii/S0304885315303048>
- Wakeham N, Rosa PFS, Wang YQ, Kang M, Fisk Z, Ronning F, Thompson JD (2016) Low-temperature conducting state in two candidate topological Kondo insulators:  $\text{SmB}_6$  and  $\text{Ce}_3\text{Bi}_4\text{Pt}_3$ . *Phys Rev B* 94:035127. doi:10.1103/PhysRevB.94.035127, <http://link.aps.org/doi/10.1103/PhysRevB.94.035127>
- Yuan HK, Chen H, Kuang AL, Tian CL, Wang JZ (2013) The spin and orbital moment of  $\text{Fe}_n$  ( $n = 2–20$ ) clusters. *J Chem Phys* 139(3):034314. doi:10.1063/1.4813611, <http://scitation.aip.org/content/aip/journal/jcp/139/3/10.1063/1.4813611>